On the structures and bonding in boron-gold alloy clusters: B6Aun− and B6Aun (n = 1−3)

Qiang Chen, Hua-Jin Zhai, Si-Dian Li, and Lai-Sheng Wang

Citation: J. Chem. Phys. **138**, 084306 (2013); doi: 10.1063/1.4792501
View online: http://dx.doi.org/10.1063/1.4792501
View Table of Contents: http://jcp.aip.org/resource/1/JCPSA6/v138/i8
Published by the American Institute of Physics.

On the structures and bonding in boron-gold alloy clusters: $B_6Au_n^-$ and B_6Au_n ($n = 1-3$)

Qiang Chen,[1] Hua-Jin Zhai,[1,2] Si-Dian Li,[1,a)] and Lai-Sheng Wang[2,b)]
[1]*Institute of Molecular Science, Shanxi University, Taiyuan 030006, China*
[2]*Department of Chemistry, Brown University, Providence, Rhode Island 02912, USA*

(Received 29 December 2012; accepted 4 February 2013; published online 26 February 2013)

Photoelectron spectroscopy and density-functional theory are combined to investigate the electronic and structural properties of a series of B−Au alloy clusters: $B_6Au_n^-$ and B_6Au_n ($n = 1-3$). Rich spectral features are observed for each species, and vibrational structures are resolved for numerous detachment transitions of B_6Au^- and $B_6Au_2^-$. Electron affinities of B_6Au_n ($n = 1-3$) are evaluated to be 2.70 ± 0.03, 2.91 ± 0.02, and 3.21 ± 0.05 eV, respectively. Global structural searches are performed for both the anions and their neutrals. The calculated electronic binding energies are compared with experimental measurements to establish the anion global-minimum structures and their corresponding neutral states. The ground-state structures of these clusters are shown to be planar or quasi-planar with an elongated B_6 core, to which the first and second Au atoms are bonded terminally and the third Au in a bridging position. All three anion clusters are π antiaromatic. Natural bond orbital analyses show that the B−Au bonding is highly covalent, providing new examples for the Au/H analogy in Au alloy clusters. © *2013 American Institute of Physics*. [http://dx.doi.org/10.1063/1.4792501]

I. INTRODUCTION

Boron-gold alloy clusters are of considerable current interest, due to the fact that boron and gold are among the rare, unique elements whose elemental clusters possess planar or quasi-planar geometries up to large sizes. Gold clusters were shown to be planar up to Au_7^+ for the cations[1] and up to Au_{12}^- for the anions.[2–4] For boron clusters,[5–16] the transitions from planar and quasi-planar to three-dimensional structures were established at B_{16}^+ for the cations,[8] at B_{20} for the neutrals,[9] and beyond B_{23}^- for the anions,[9–16] where the exact size for the latter is still open. The rich chemical bonding properties of boron[17,18] are primarily attributed to its intrinsic electron deficiency, which results in three-center two-electron (3c-2e) bonds in boranes[19] and aromaticity and antiaromaticity in boron clusters.[16] Thus, interesting cluster structures are anticipated for the B−Au alloy system.

Owing to the relativistic effects,[20] Au has the highest electron affinity (EA) (2.3086 eV) of any element other than the halogens and the highest electronegativity (2.4 in the Pauling scale) of all metals as well. The high EA of Au leads to auride compounds such as Cs^+Au^-, in which Au behaves like a halogen.[21] Gold has also been found to form strong covalent bonds,[22,23] exemplified by the Au/H isolobal analogy in binary Au clusters.[24–30] The concept of Au/H analogy is an extension of the well-established isolobal analogy between a gold phosphine ($AuPR_3$) unit and a hydrogen atom, which has helped the elucidation of the structures and bonding in a variety of ligated Au compounds.[31] Gas-phase Si−Au alloy clusters, such as $SiAu_4$, $SiAu_n$ ($n = 2, 3$), Si_2Au_n ($n = 2, 4$), and Si_3Au_3, were shown to be similar in structures and bonding to SiH_4, SiH_n ($n = 2, 3$), Si_2H_n ($n = 2, 4$), and Si_3H_3, respectively, demonstrating the Au/H analogy in the Si−Au alloy system.[24]

Only a limited number of B−Au alloy clusters have been studied lately.[25–30] The $B_7Au_2^-$ cluster[25] was first shown to possess structure and bonding similar to $B_7H_2^-$,[32] and the B−Au bonding was revealed to be highly covalent as well, analogous to the B−H bonding. A subsequent study[27] showed that the $B_{10}Au^-$ cluster is similar to $B_{10}H^-$ in terms of structure and bonding. The Au/H analogy also motivated theoretical studies on B−Au alloy clusters, such as $BAu_n^{0/-}$ ($n = 1-4$) and $B_2Au_n^{0/-}$ ($n = 1-5$).[28,29] Furthermore, a series of deltahedral *closo*-auro-boranes ($B_nAu_n^{2-}$) were computed,[30] which are analogous to the well-known *closo*-boranes $B_nH_n^{2-}$ ($n = 5-12$). These studies on Si−Au and B−Au alloy clusters suggest that the Au/H analogy is a rather general concept and may be further developed, where Au serves as a monovalent σ ligand akin to H.

In the present contribution, we report a combined photoelectron spectroscopy (PES) and density-functional theory (DFT) study on a series of B−Au alloy clusters: $B_6Au_n^-$ and B_6Au_n ($n = 1-3$). The B_6^- and B_6 clusters[11] are the smallest that exhibit double (π and σ) antiaromaticity with an elongated overall shape. In $B_6Au_n^-$ and B_6Au_n ($n = 1-3$) clusters, the Au ligands should use some of the σ molecular orbitals (MOs) for Au–B bonding, while leaving the π framework intact. Elucidating the structural evolution and bonding changes in these clusters is important in understanding the B−Au alloy cluster system. The present study shows that $B_6Au_n^-$ and B_6Au_n ($n = 1-3$) all adopt structures with an elongated B_6 core. The first two Au atoms are bonded terminally to B_6 and the third Au atom occupies a bridging

a)Electronic mail: lisidian@sxu.edu.cn.
b)Electronic mail: Lai-Sheng_Wang@brown.edu.

position. The three anion clusters are all π antiaromatic, consistent with their elongated shapes.

II. EXPERIMENTAL AND COMPUTATIONAL METHODS

A. Photoelectron spectroscopy

The experiment was carried out using a magnetic-bottle-type PES apparatus equipped with a laser vaporization cluster source, details of which were described previously.[33,34] Briefly, $B_6Au_n^-$ ($n = 1-3$) clusters were produced by laser vaporization of an Au/B mixed disk target (^{10}B isotope enriched, 99.75%) in the presence of a helium carrier gas. Cluster anions were analyzed using a time-of-flight mass spectrometer, and the $B_6Au_n^-$ ($n = 1-3$) species were each mass-selected and decelerated before being photodetached. Three detachment photon energies were used in the current experiment: 355 nm (3.496 eV) and 266 nm (4.661 eV) from an Nd:YAG laser and 193 nm (6.424 eV) from an ArF excimer laser. Effort was made to choose colder clusters (that is, those with long resident times in the nozzle) for photodetachment, which was shown previously to be critical for obtaining high quality PES data.[35] Photoelectrons were collected at nearly 100% efficiency by the magnetic bottle and analyzed in a 3.5 m long electron flight tube. The PES spectra were calibrated using the known spectra of Rh^- and Au^-. The energy resolution of the apparatus was $\Delta E_k/E_k \sim 2.5\%$, that is, ~25 meV for 1 eV kinetic energy electrons.

B. Computational methods

The DFT structural searches were performed using the Coalescence-Kick (CK) global minimum search program,[14,36] initially at the PBE/LanL2DZ level.[37,38] The top 15 low-lying candidate structures were then fully optimized at the PBE/Au/SDD/B/6-311++G(d,p) level.[37] Frequency calculations were done to confirm that the reported structures are true minima. Wavefunction stability was tested for $B_6Au_n^-$ and B_6Au_n ($n = 1-3$), and the wavefunctions are stable under the perturbations considered. Excitation energies of the neutral clusters were calculated using the time-dependent DFT (TDDFT) method[39] at the anion ground-state geometries. Single-point CCSD(T) calculations[40] were done at the PBE/Au/SDD/B/6-311++G(d,p) geometries to further evaluate the relative energies of the top five low-lying structures and to refine the ground-state vertical detachment energies (VDEs). All calculations were done using the GAUSSIAN 09 package.[41]

III. EXPERIMENTAL RESULTS

A. B_6Au^-

The PES spectra of B_6Au^- are shown in Fig. 1. The 355 nm spectrum (Fig. 1(a)) reveals a broad shoulder, X (VDE: 2.78 eV; Table I)[42] and an intense and sharp peak A (VDE: 3.05 eV). At 266 nm, peak A is revealed to be the first peak of a vibrational progression (Fig. 1(b)). The ground-state band X is also better defined in the 266 nm spectrum. Since

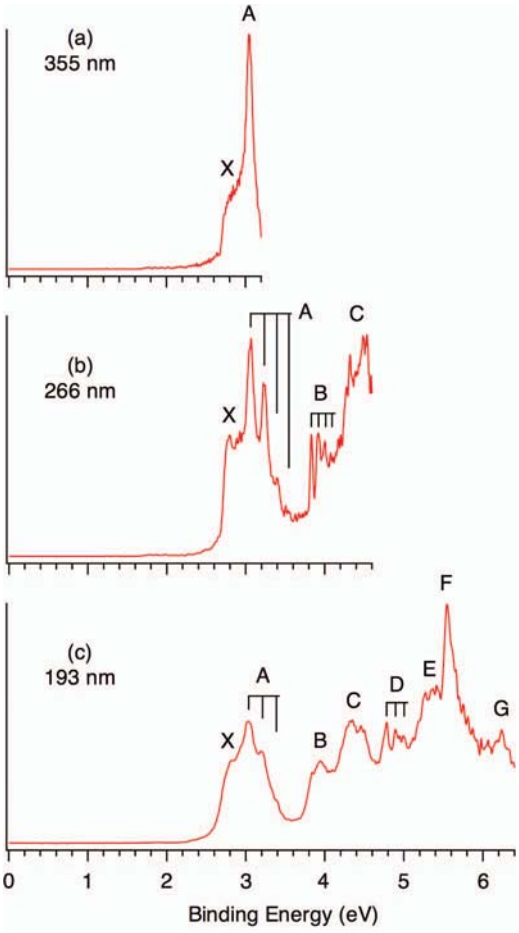

FIG. 1. Photoelectron spectra of B_6Au^- at (a) 355 nm (3.496 eV), (b) 266 nm (4.661 eV), and (c) 193 nm (6.424 eV). The vertical lines represent vibrational structures.

the vibrational structures for band X are not clearly resolved, the adiabatic detachment energy (ADE) is estimated by drawing a straight line along the leading edge and then adding the instrumental resolution to the intersection with the binding energy axis. The ADE thus evaluated is 2.70 ± 0.03 eV, which is also the EA of neutral B_6Au cluster. The vibrational progression for band A yields a spacing of 1400 ± 30 cm^{-1}. Band B (VDE: 3.92 eV) also exhibits a vibrational progression, with a smaller spacing of 720 cm^{-1}. Centering at ~4.4 eV, band C appears broad with discernible vibrational structures. The 193 nm spectrum (Fig. 1(c)) shows four more bands at higher binding energies: D, E, F, G at 4.78, 5.35, 5.55, and 6.24 eV, respectively. Among these, band D is vibrationally resolved with a spacing of 880 cm^{-1} and band F is intense and sharp.

B. $B_6Au_2^-$

At 355 and 266 nm, the ground-state band X of $B_6Au_2^-$ is vibrationally resolved with a spacing of 1350 cm^{-1} (Fig. 2). The sharp peak at 2.91 eV is the 0−0 transition and defines the ground state ADE and VDE. The weak peak at 2.74 eV is assigned to a vibrational hot band. Two broad bands A (VDE: 3.84 eV) and B (VDE: 4.21 eV) are also observed at 266 nm. At 193 nm, three additional, vibrationally resolved

TABLE I. Experimental adiabatic and vertical detachment energies (ADEs and VDEs; in eV) and vibrational frequencies (in cm^{-1}) from the photoelectron spectra of $B_6Au_n^-$ ($n = 1-3$), as compared to the calculated ADEs and VDEs.

Species	Feature	ADE (expt.)[a]	VDE (expt.)[a]	Vib. freq. (expt.)[a,b]	Final state[c]	ADE (theor)[d]	VDE (theor)[d]
B_6Au^-	X	2.70 (3)[e]	2.78 (3)[f]		$^2A''$	2.82[g]	3.12[g]
	A		3.05 (2)	1400 (30)	$^2A''$		3.20
	B		3.92 (2)	720 (30)	$^2A'$		3.92
	C		∼4.4		$^2A'$		4.26
	D		4.78 (3)	880 (30)	$^2A'$		4.69
	E		5.35 (5)		$^2A'$		4.89
	F		5.55 (3)		$^2A'', ^2A'$		5.19, 5.19
					$^2A''$		5.61
	G		6.24 (3)		$^2A', ^2A''$		6.29, 6.34
$B_6Au_2^-$	X	2.91 (2)[e]	2.91 (2)	1350 (30)	^1A_g	3.04[g]	3.13[g]
	A		3.84 (5)		$^3B_g, ^1B_g$		3.62, 3.79
	B		4.21 (5)		$^3A_u, ^1A_u$		3.87, 4.25
					$^3B_g, ^1B_g$		4.48, 4.81
	C		4.87 (3)	930 (50)	$^3A_u, ^1A_u$		4.66, 4.83
					$^3B_g, ^1B_g$		4.68, 4.95
	D		5.23 (3)	960 (50)	$^3B_u, ^1B_u$		5.19, 5.42
	E		5.58 (2)	1160 (50)	$^3A_g, ^1A_g$		5.35, 5.42
					$^3B_u, ^1B_g$		5.35, 5.43
					$^3B_g, ^1A_u$		5.35, 5.43
					$^3A_u, ^1B_u$		5.35, 5.80
					$^3A_u, ^1A_u$		6.26, 6.38
$B_6Au_3^-$	X	3.21 (5)[e]	3.43 (5)		^2A	2.97[g]	3.35[g]
	A		3.93 (5)		$^2A, ^2A$		3.74, 3.97
	B		4.33 (5)		$^2A, ^2A$		4.52, 4.55
	C		4.94 (3)		^2A		4.98
	D		5.35 (2)		$^2A, ^2A$		5.12, 5.12
	E		5.58 (2)		$^2A, ^2A$		5.41, 5.42
					^2A		5.69
	F		6.13 (5)		^2A		6.06

[a]Numbers in the parentheses represent experimental uncertainties in the last digits.
[b]Symmetric vibrational modes for the neutral cluster.
[c]For B_6Au^- (C_s, $^3A''$), transitions to quartet final states cannot be calculated at the TDDFT level using GAUSSIAN 09. At the OVGF level, the first few VDEs are predicted at 2.90 ($^2A''$), 3.20 ($^2A''$), 3.70 ($^4A'$), 4.25 ($^4A'$), and 4.44 ($^2A'$).
[d]Calculated at the PBE/Au/SDD/B/6-311++G(d,p) level.
[e]Electron affinity of the neutral cluster.
[f]See Ref. 42.
[g]Ground-state ADEs/VDEs at the CCSD(T)//PBE/Au/SDD/B/6-311++G(d,p) level are 2.56/2.97, 2.61/2.77, and 2.71/3.15 eV for $B_6Au_n^-$ ($n = 1-3$), respectively.

bands (C, D, and E) are observed. Their VDEs are 4.87, 5.23, and 5.58 eV, and their vibrational frequencies are 930, 960, and 1160 cm^{-1}, respectively. Note that band E is the most intense transition at 193 nm.

C. $B_6Au_3^-$

The PES spectra of $B_6Au_3^-$ are shown in Fig. 3 at two detachment energies. The bands are all broad without vibrational resolution, in contrast to those of B_6Au^- and $B_6Au_2^-$. The 266 nm spectrum (Fig. 3(a)) exhibits three bands, X, A, and B, at VDEs of 3.43, 3.93, and 4.33 eV, respectively. The ground-state ADE is estimated from the onset of band X to be 3.21 eV. The 193 nm spectrum (Fig. 3(b)) further reveals four well-defined bands at higher binding energies: C (VDE: 4.94 eV), D (VDE: 5.35 eV), E (VDE: 5.58 eV), and F (VDE: 6.13 eV). The D and E bands show higher intensities, similar to the prominent band F for B_6Au^- (Fig. 1) and band E for $B_6Au_2^-$ (Fig. 2).

IV. THEORETICAL RESULTS

All low-lying cluster structures for $B_6Au_n^-$ and B_6Au_n ($n = 1-3$) are summarized in Figs. S1–S6 in the supplementary material.[43] These structures were obtained initially using the CK global minimum search method at the PBE/LanL2DZ level and their relative energies subsequently refined at the PBE/Au/SDD/B/6-311++G(d,p) and CCSD(T)//PBE/Au/SDD/B/6-311++G(d,p) levels. The optimized anion global-minimum structures (**1**–**3**) for $B_6Au_n^-$ ($n = 1-3$) and their corresponding neutral global-minimum structures (**4**–**6**) at the PBE/Au/SDD/B/6-311++G(d,p) level are shown in Fig. 4, which are all based on the double-chain, elongated B_6 motif.[11] Detailed B–B and B–Au bond distances for structures **1**–**6** are shown in Fig. S10 in the supplementary material.[43]

A. B_6Au^- and B_6Au

The global minimum structure for B_6Au^- is a triplet state **1** (C_s, $^3A''$) with the Au atom bonded terminally to

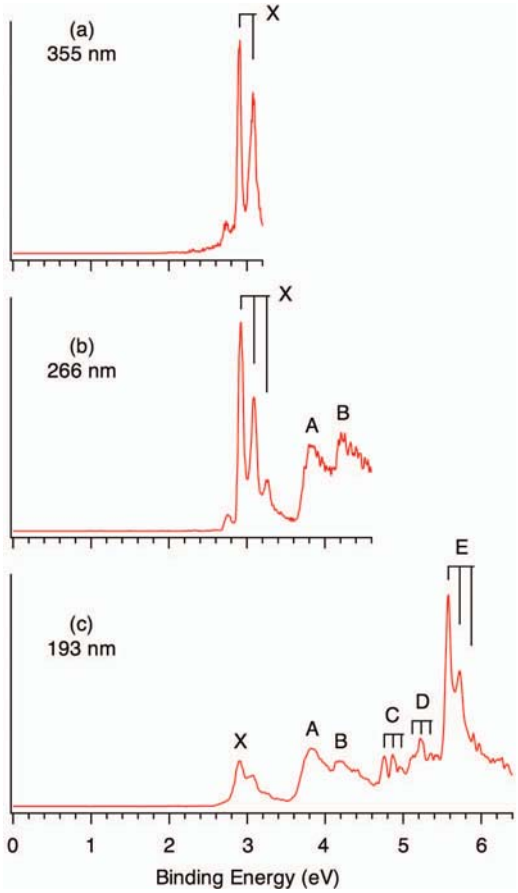

FIG. 2. Photoelectron spectra of $B_6Au_2^-$ at (a) 355 nm, (b) 266 nm, and (c) 193 nm. The vertical lines represent vibrational structures. The minor peak at 2.74 eV is assigned to a hot band transition.

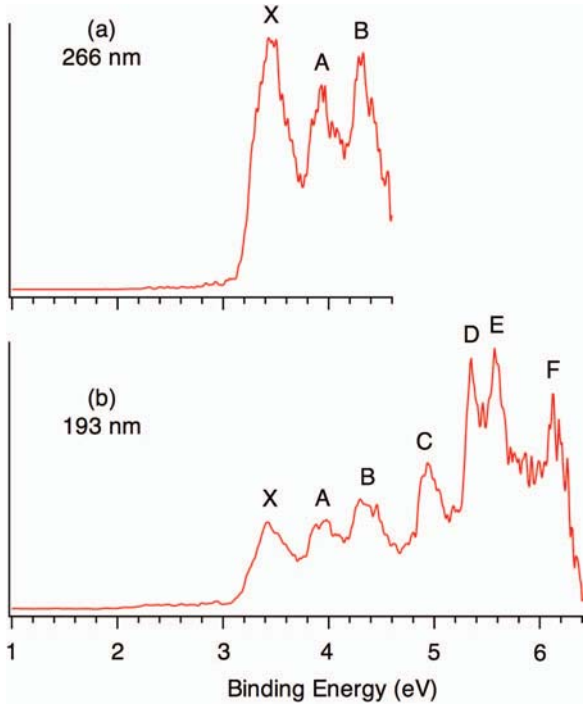

FIG. 3. Photoelectron spectra of $B_6Au_3^-$ at (a) 266 nm and (b) 193 nm.

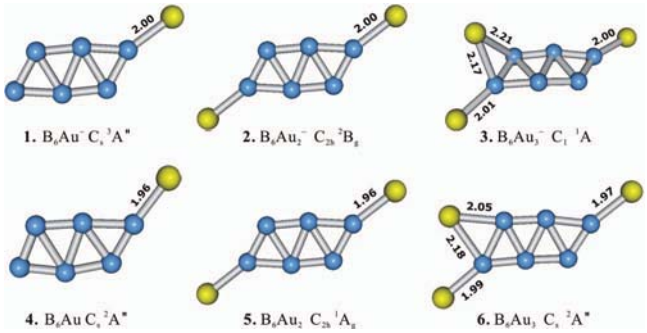

FIG. 4. Optimized anion global-minimum structures (**1**−**3**) for $B_6Au_n^-$ (n = 1−3) clusters and their corresponding neutral structures (**4**−**6**) at the PBE/Au/SDD/B/6-311++G(d,p) level. The B−Au bond distances are labeled.

an apex of the B_6 motif (Fig. 4). This is closely followed by the corresponding singlet state **7** (C_1, ^{1}A; see Fig. S1 in the supplementary material),[43] which is higher in energy by 1.40 kcal/mol at the CCSD(T) level. Alternative structures are at least 8 kcal/mol above the global minimum. Corresponding to anion global-minimum structure **1**, the neutral state **4** (C_s, $^2A''$) (Fig. 4) is the global minimum for the B_6Au neutral, with alternative structures being at least 11 kcal/mol higher in energy (Fig. S2 in the supplementary material).[43]

B. $B_6Au_2^-$ and B_6Au_2

Our structural search reveals that **2** (C_{2h}, ^2B_g) is clearly the global-minimum structure for $B_6Au_2^-$ (Fig. 4), and alternative structures are at least ∼8 kcal/mol higher in energy at both the PBE and CCSD(T) levels; see Fig. S3 in the supplementary material.[43] Structure **2** has two Au atoms attached terminally to the B_6 motif in a *trans* fashion, whose corresponding neutral structure **5** (C_{2h}, ^1A_g) (Fig. 4) turns out to be the global minimum for B_6Au_2. A low-lying structure **8** (C_{2v}, $^1A_1$; see Fig. S4 in the supplementary material)[43] is also located for B_6Au_2, which contains an incomplete hexagonal wheel-like boron motif, with two Au atoms attached terminally.

C. $B_6Au_3^-$ and B_6Au_3

Our structural searches reveal that $B_6Au_3^-$ and B_6Au_3 can be constructed based upon $B_6Au_2^-$ and B_6Au_2, with the third Au atom preferring a bridging site; see Figs. S5−S6 in the supplementary material.[43] The global minimum for $B_6Au_3^-$ is **3** (C_1, ^{1}A) (Fig. 4), in which the bridging Au atom is significantly out-of-plane. Alternative anion structures are at least ∼7 kcal/mol higher in energy. The global minimum for the B_6Au_3 neutral is **6** (C_s, $^2A''$) (Fig. 4), similar to the anion global minimum **3** except that structure **6** is completely planar. A low-lying neutral structure **9** (C_s, $^2A''$; see Fig. S6 in the supplementary material),[43] in which the third Au atom occupies a different bridging position, is ∼2.5 kcal/mol higher in energy at both the PBE and CCSD(T) levels.

V. COMPARISON BETWEEN EXPERIMENT AND THEORY

The global-minimum structures (**1**−**3**) for $B_6Au_n^-$ (n = 1−3) are quite stable and should be responsible for the observed PES spectra, except for B_6Au^- where a low-lying structure **7** (Fig. S1 in the supplementary material)[43] may potentially be populated as a minor isomer. Similarly, the neutral global-minimum structures (**4**−**6**) are all very stable relative to the second low-lying isomer in each case. The calculated VDEs and ground-state ADEs on the basis of structures **1**−**3** are given in Table I. Due to the high density of electronic states, only some general comparisons will be made with the experimental data, instead of detailed peak-by-peak spectral assignments.

The PBE calculated ground-state VDEs from **1**−**3**, which are 3.12, 3.13, and 3.35 eV, respectively (Table I), are compared to the experimental data of 2.78 (see Ref. 42), 2.91, and 3.43 eV. Similarly, the calculated ground-state ADEs are 2.82, 3.04, and 2.97 eV, respectively, which are compared to the experimental measurements of 2.70, 2.91, and 3.21 eV. The errors are thus typically 0.1−0.3 eV. The CCSD(T) single-point calculations result in similar ground-state VDEs, 2.97, 2.77, and 3.15 eV for **1**−**3**, respectively (Table I). In particular, the values for **1** and **2**, when compared to the PBE data, are in closer agreement with experiment. The CCSD(T) results also reproduces the ADEs very well for **1** and **2**, although its performance with respect to the ADE/VDE for **3** is less satisfactory. Comparisons of PBE and CCSD(T) data with experiment thus suggest that PBE performs rather well for the B−Au binary clusters. It is worth noting that the energetics for the top five low-lying structures of $B_6Au_n^-$ and B_6Au_n (n = 1−3) from PBE and CCSD(T) calculations are remarkably consistent with each other; see Figs. S1−S6 in the supplementary material.[43]

The calculated VDE patterns for structures **1**−**3** correlate well with the observed PES bands, allowing qualitative spectral assignments as given in Table I. The validity of the assignments is confirmed further by the dominant PES bands in the ∼5.3−5.6 eV regime in each case: band F at 5.55 eV for B_6Au^-; band E at 5.58 eV for $B_6Au_2^-$; and bands D/E at 5.35/5.58 eV for $B_6Au_3^-$. These bands each involve multiple nearly degenerate electronic transitions, and correspond to detachment transitions from MOs mainly of Au 5*d* characters and thus possess larger photodetachment cross sections relative to the boron based orbitals, as observed experimentally.

It should be pointed out that the low-lying structure **7** for B_6Au^- (see Fig. S1 in the supplementary material)[43] is unlikely to make major contributions to the PES spectra, because it has only one predicted electronic transition in the 2.5−3.5 eV binding energy regime (PBE: ADE 2.63 eV; VDE 2.76 eV), while the experimental spectra clearly show two transitions in this regime (Fig. 1). The contribution from structure **7**, if any, may be minor and are likely to be buried in the PES bands from the global-minimum structure **1**.

We also note that for the open-shell B_6Au^- (**1**) and $B_6Au_2^-$ (**2**) clusters, their final neutral excited states include both high-spin and low-spin states (quartets/doublets for B_6Au and triplets/singlets for B_6Au_2) and the high-spin states are anticipated to dominate the PES spectra. However, the VDEs for quartet final states of B_6Au, which contribute to the observed PES spectra beyond band B (Fig. 1), cannot be calculated at the TDDFT level using the GAUSSIAN 09 program. To address this technical issue, supplementary OVGF calculations were performed.[44,45] The predicted first few VDEs at the OVGF level are 2.90 ($^2A''$), 3.20 ($^2A''$), 3.70 ($^4A'$), 4.25 ($^4A'$), and 4.44 eV ($^2A'$), which are consistent with the experimental bands X−C (Fig. 1).

VI. DISCUSSION

A. Structure and bonding: Peripheral two-center two-electron (2c-2e) bonds versus delocalized π and σ bonds

Based on comparisons between experiment and theory, the global-minimum structures (**1**−**3**; Fig. 4) for $B_6Au_n^-$ (n = 1−3) anion clusters are established, as are their corresponding neutral final states (**4**−**6**). All these alloy cluster species are based on the double-chain B_6 motif, where the first and second Au atoms are attached terminally to the apex sites in B_6Au^-/B_6Au and $B_6Au_2^-/B_6Au_2$, while the third Au atom is attached to a bridging site in $B_6Au_3^-/B_6Au_3$. The global minima of $B_6Au_n^-$ and B_6Au_n clusters are similar to their B-H counterparts.[46] They also follow the structural trend of the $B_7Au_2^-$ (Ref. 25) and $B_nH_2^-$ clusters.[32,47]

Chemical bonding in the $B_6Au_n^-$ and B_6Au_n (n = 1−3) system can be understood starting from that in B_6^{2-}.[11] The B_6^{2-} dianion is built via the fusion of two doubly (π and σ) aromatic B_3^- clusters,[12] resulting in a doubly antiaromatic B_6^{2-} species with 4π and 4σ delocalized electrons, which is consistent with its elongated shape. The remaining 12 valence electrons can be localized as six peripheral 2c-2e bonds, one on each edge.

As shown in Fig. 5, the two delocalized π MOs retain intact in $B_6Au_n^-$ (n = 1−3): HOMO−1 (half occupied) and HOMO−6 in B_6Au^- (**1**), HOMO (half occupied) and HOMO−6 in $B_6Au_2^-$ (**2**), and HOMO and HOMO−5 in $B_6Au_3^-$ (**3**). Such orbital occupations render π antiaromaticity for these binary clusters. For delocalized σ MOs, two remain in B_6Au^- (**1**; half-occupied HOMO and HOMO−3), rendering this cluster σ antiaromaticity as well. One of the delocalized σ MOs is used to form B−Au bond for the second and third Au, leaving only one delocalized σ MO in $B_6Au_2^-$

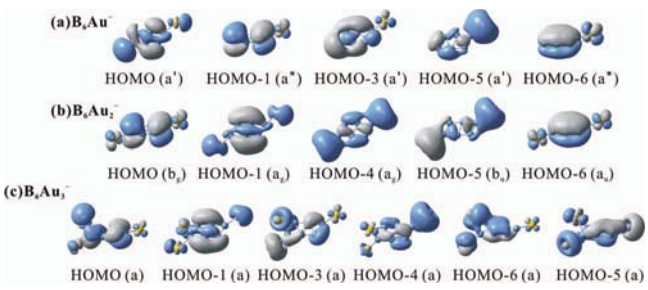

FIG. 5. Pictures of selected molecular orbitals for the global-minimum structures of $B_6Au_n^-$ (n = 1−3). These include orbitals that are responsible for the delocalized π and σ bonding and the terminal and bridging B−Au bonds.

(**2**; HOMO−1) and $B_6Au_3^-$ (**3**; HOMO−1), which renders these two clusters σ aromaticity according to the Hückel ($4n + 2$) rule. Hence, B_6Au^- remains doubly (σ and π) antiaromatic, whereas $B_6Au_2^-$ and $B_6Au_3^-$ show conflicting aromaticity (π antiaromatic and σ aromatic).[48] We note that the delocalized σ MO in $B_6Au_2^-$ (HOMO−1) and $B_6Au_3^-$ (HOMO−1) involve almost no contributions from the two apex sites that are bonded to Au, suggesting that these MOs are primarily responsible for bonding within the central four B atoms.

Other MOs shown in Fig. 5 are responsible for B−Au bonding, which may be characterized as 2c-2e bonds for the terminal Au (HOMO−5 in B_6Au^-, HOMO−4 and HOMO−5 in $B_6Au_2^-$, and HOMO−3 and HOMO−4 in $B_6Au_3^-$) and a 3c-2e bond for the bridging Au (HOMO−6 in $B_6Au_3^-$). Among the additional MOs (not shown in Fig. 5; see Figs. S7−S9 in the supplementary material),[43] those responsible for the Au d^{10} lone-pairs can be readily identified, thus leaving six, six, and five MOs that are roughly attributed to the peripheral B−B σ bonding in $B_6Au_n^-$ ($n = 1-3$), respectively.[49] Note that the number of σ MOs in $B_6Au_3^-$ is one less than the number of edges, hinting that as expected, the peripheral B−B σ framework is no longer complete and a peripheral B−B σ bond is broken upon Au attachment to form the B−Au−B 3c-2e σ bond.

B. On the vibrational structures

A number of PES bands for B_6Au^- (A, B, and D; Fig. 1) and $B_6Au_2^-$ (X, C, D, and E; Fig. 2) are vibrationally resolved, although none for $B_6Au_3^-$ (Fig. 3). This observation is consistent with the fact that $B_6Au_3^-/B_6Au_3$ (**3** and **6**; Fig. 4) appear to be more floppy with large anion-to-neutral structural changes. Vibrational analysis can be performed for B_6Au (**4**) and B_6Au_2 (**5**). While the calculated vibrational modes are for the neutral ground states, they do provide a rough guide for assignments of the observed vibrational structures, which are mostly for the excited states. Briefly, PBE calculated symmetric ground-state vibrational modes are 1349 (central B_4 breathing), 833 (B_6 breathing), and 665 cm^{-1} (B−Au stretching) for B_6Au, and 1363 (central B_4 breathing), 1250 (central B_4 stretching), and 1018 cm^{-1} (B_6 breathing) for B_6Au_2.

On the basis of these values, it seems appropriate to assign the observed modes as follows: Band A of B_6Au^- (1400 cm^{-1}) and band X of $B_6Au_2^-$ (1350 cm^{-1}) for central B_4 breathing, band D of B_6Au^- (880 cm^{-1}) and bands C/D of $B_6Au_2^-$ (930, 960 cm^{-1}) for B_6 breathing, band E of $B_6Au_2^-$ (1160 cm^{-1}) for central B_4 stretching, and band B of B_6Au^- (720 cm^{-1}) for B−Au stretching. The above assignments are also in line with the nature of the MOs from which the electron is detached. For example, both band A of B_6Au^- and band X of $B_6Au_2^-$ are associated with the partly antibonding π MO, whose electron detachment should activate the central B_4 breathing; whereas band B of B_6Au^- involves certain B−Au bonding character (HOMO−2), activating the B−Au stretching upon electron removal. The vibrational structures thus provide further structural proof for the alloy clusters.

C. B−Au bond covalency and Au/H analogy

There have been a limited number of prior studies on the B−Au alloy clusters.[25–30] The current $B_6Au_n^-$ and B_6Au_n ($n = 1-3$) series offers new examples to elucidate the nature of the B−Au bonding. As shown in Fig. 4, Au atoms are attached to the B_6 motif either terminally or in a bridging fashion. The B−Au σ bonds in $B_6Au_n^-$ ($n = 1-3$) can be easily identified from the MOs (Fig. 5): HOMO−5 in B_6Au^-, HOMO−4 and HOMO−5 in $B_6Au_2^-$, and HOMO−3, HOMO−4, and HOMO−6 in $B_6Au_3^-$. Note that the terminal B−Au bond distances are nearly identical along the series, 2.00−2.01 Å for the anions and 1.96−1.99 Å for the neutrals (Fig. 4), which are typical for B−Au single bond.[30] The bridging B−Au distances are much longer, consistent with a 3c-2e B−Au−B bond. Natural bond orbital (NBO) analysis confirms the highly covalent B−Au bonding,[50] with the Wiberg bond orders of 1.04, 1.05, 1.00/1.05, 1.12, 1.19, and 1.03/1.13 for the terminal bonds in **1**−**6**, and 0.61/0.50 and 0.49/0.65 for the bridging bonds in **3** and **6**, respectively.

It is interesting to compare $B_6Au_n^-$ and B_6Au_n ($n = 1-3$) with relevant B−H clusters.[46,51,52] The global-minimum structure of B_6Au^- (**1**) and its neutral state B_6Au (**4**) are similar to that of $B_6H^{+/-}$,[46,51] whereas the global-minimum structures of $B_6Au_2^-$ (**2**) and B_6Au_2 (**5**) are identical to those of $B_6H_2^-$ and B_6H_2.[46,52] In fact, the first nine bands in the simulated PES spectrum[52] of $B_6H_2^-$ are quite similar to those calculated for $B_6Au_2^-$ (Table I). Our calculations and those in Ref. 46 also indicate that $B_6H_3^-$ possesses C_1 ground-state structure with a bridging Au, analogous to $B_6Au_3^-$ (**3**). These observations offer further examples for the Au/H analogy in Au alloy clusters, due to the high electronegativity of Au as a result of strong relativistic effects.[20] The B−Au bonding in $B_6Au_n^-$ and B_6Au_n ($n = 1-3$) also closely parallels the B−(BO) bonding in boron oxide clusters[53–55] in terms of the terminal and bridging bonds, because Au and BO are both monovalent σ ligands analogous to H.

VII. CONCLUSIONS

We have combined photoelectron spectroscopy and density-functional theory calculations to investigate the electronic and structural properties and chemical bonding in a series of B−Au alloy clusters: $B_6Au_n^-$ and B_6Au_n ($n = 1-3$). Rich spectral features are observed for the anion clusters and vibrational structures resolved for numerous transitions for B_6Au^- and $B_6Au_2^-$. The electron affinities of B_6Au_n ($n = 1-3$) are determined to be 2.70 ± 0.03, 2.91 ± 0.02, and 3.21 ± 0.05 eV, respectively. Extensive structural searches and electronic binding energy calculations allow detailed comparisons with the experimental data, establishing the anion global-minimum structures and their corresponding neutral states. These planar or quasi-planar alloy clusters are shown to possess an elongated B_6 core. The first and second Au atoms are shown to be attached terminally each on an apex site, whereas the third Au atom occupies a bridging position. All three anion clusters are π antiaromatic. Natural bond orbital analyses reveal that B−Au bonding is highly covalent,

providing new examples for the Au/H analogy in Au alloy clusters.

ACKNOWLEDGMENTS

S.D.L. thanks Professor Alexander I. Boldyrev for the Coalescence-Kick global minimum search program. The experimental work at Brown was supported by the National Science Foundation (DMR-0904034 to L.S.W.) and the computational work at Shanxi was supported by the National Natural Science Foundation of China (Grant No. 20873117 to S.D.L.).

[1] S. Gilb, P. Weis, F. Furche, R. Ahlrichs, and M. M. Kappes, J. Chem. Phys. **116**, 4094 (2002).
[2] F. Furche, R. Ahlrichs, P. Weis, C. Jacob, S. Gilb, T. Bierweiler, and M. M. Kappes, J. Chem. Phys. **117**, 6982 (2002).
[3] H. Hakkinen, B. Yoon, U. Landman, X. Li, H. J. Zhai, and L. S. Wang, J. Phys. Chem. A **107**, 6168 (2003).
[4] M. P. Johansson, A. Lechtken, D. Schooss, M. M. Kappes, and F. Furche, Phys. Rev. A **77**, 053202 (2008).
[5] H. Kato, K. Yamashita, and K. Morokuma, Chem. Phys. Lett. **190**, 361 (1992); J. M. L. Martin, J. P. Francois, and R. Gijbels, *ibid.* **189**, 529 (1992); R. Kawai and J. H. Weare, *ibid.* **191**, 311 (1992).
[6] I. Boustani, Int. J. Quantum Chem. **52**, 1081 (1994); Phys. Rev. B **55**, 16426 (1997).
[7] A. Ricca and C. W. Bauschlicher, Jr., Chem. Phys. **208**, 233 (1996); F. L. Gu, X. M. Yang, A. C. Tang, H. J. Jiao, and P. v. R. Schleyer, J. Comput. Chem. **19**, 203 (1998); J. E. Fowler and J. M. Ugalde, J. Phys. Chem. A **104**, 397 (2000); J. I. Aihara, H. Kanno, and T. Ishida, J. Am. Chem. Soc. **127**, 13324 (2005); J. O. C. Jimenez-Halla, R. Islas, T. Heine, and G. Merino, Angew. Chem., Int. Ed. **49**, 5668 (2010); G. Martinez-Guajardo, A. P. Sergeeva, A. I. Boldyrev, T. Heine, J. M. Ugalde, and G. Merino, Chem. Commun. **47**, 6242 (2011).
[8] E. Oger, N. R. M. Crawford, R. Kelting, P. Weis, M. M. Kappes, and R. Ahlrichs, Angew. Chem., Int. Ed. **46**, 8503 (2007).
[9] B. Kiran, S. Bulusu, H. J. Zhai, S. Yoo, X. C. Zeng, and L. S. Wang, Proc. Natl. Acad. Sci. U.S.A. **102**, 961 (2005).
[10] A. P. Sergeeva, Z. A. Piazza, C. Romanescu, W. L. Li, A. I. Boldyrev, and L. S. Wang, J. Am. Chem. Soc. **134**, 18065 (2012).
[11] A. N. Alexandrova, A. I. Boldyrev, H. J. Zhai, L. S. Wang, E. Steiner, and P. W. Fowler, J. Phys. Chem. A **107**, 1359 (2003).
[12] H. J. Zhai, L. S. Wang, A. N. Alexandrova, A. I. Boldyrev, and V. G. Zakrzewski, J. Phys. Chem. A **107**, 9319 (2003).
[13] H. J. Zhai, L. S. Wang, A. N. Alexandrova, and A. I. Boldyrev, J. Chem. Phys. **117**, 7917 (2002).
[14] A. P. Sergeeva, B. B. Averkiev, H. J. Zhai, A. I. Boldyrev, and L. S. Wang, J. Chem. Phys. **134**, 224304 (2011).
[15] H. J. Zhai, A. N. Alexandrova, K. A. Birch, A. I. Boldyrev, and L. S. Wang, Angew. Chem., Int. Ed. **42**, 6004 (2003); H. J. Zhai, B. Kiran, J. Li, and L. S. Wang, Nat. Mater. **2**, 827 (2003); A. N. Alexandrova, A. I. Boldyrev, H. J. Zhai, and L. S. Wang, J. Phys. Chem. A **108**, 3509 (2004); Inorg. Chem. **43**, 3552 (2004); J. Chem. Phys. **122**, 054313 (2005); A. P. Sergeeva, D. Yu. Zubarev, H. J. Zhai, A. I. Boldyrev, and L. S. Wang, J. Am. Chem. Soc. **130**, 7244 (2008); W. Huang, A. P. Sergeeva, H. J. Zhai, B. B. Averkiev, L. S. Wang, and A. I. Boldyrev, Nat. Chem. **2**, 202 (2010); Z. A. Piazza, W. L. Li, C. Romanescu, A. P. Sergeeva, L. S. Wang, and A. I. Boldyrev, J. Chem. Phys. **136**, 104310 (2012).
[16] For a review on all-boron aromatic clusters, see A. N. Alexandrova, A. I. Boldyrev, H. J. Zhai, and L. S. Wang, Coord. Chem. Rev. **250**, 2811 (2006).
[17] N. N. Greenwood and A. Earnshaw, *Chemistry of the Elements*, 2nd ed. (Butterworth-Heinemann, Oxford, 1997).
[18] F. A. Cotton, G. Wilkinson, C. A. Murrillo, and M. Bochmann, *Advanced Inorganic Chemistry*, 6th ed. (Wiley, New York, 1999).
[19] W. N. Lipscomb, *Boron Hydrides* (Benjamin, New York, 1963); W. N. Lipscomb, Science **196**, 1047 (1977).
[20] P. Pyykko, Chem. Rev. **88**, 563 (1988).
[21] P. Pyykko, Angew. Chem., Int. Ed. **41**, 3573 (2002).
[22] H. J. Zhai, C. Bürgel, V. Bonacic-Koutecky, and L. S. Wang, J. Am. Chem. Soc. **130**, 9156 (2008); X. B. Wang, Y. L. Wang, J. Yang, X. P. Xing, J. Li, and L. S. Wang, *ibid.* **131**, 16368 (2009).
[23] L. S. Wang, Phys. Chem. Chem. Phys. **12**, 8694 (2010).
[24] B. Kiran, X. Li, H. J. Zhai, L. F. Cui, and L. S. Wang, Angew. Chem., Int. Ed. **43**, 2125 (2004); X. Li, B. Kiran, and L. S. Wang, J. Phys. Chem. A **109**, 4366 (2005); B. Kiran, X. Li, H. J. Zhai, and L. S. Wang, J. Chem. Phys. **125**, 133204 (2006).
[25] H. J. Zhai, L. S. Wang, D. Yu. Zubarev, and A. I. Boldyrev, J. Phys. Chem. A **110**, 1689 (2006).
[26] D. Yu. Zubarev, A. I. Boldyrev, J. Li, H. J. Zhai, and L. S. Wang, J. Phys. Chem. A **111**, 1648 (2007).
[27] H. J. Zhai, C. Q. Miao, S. D. Li, and L. S. Wang, J. Phys. Chem. A **114**, 12155 (2010).
[28] D. Z. Li and S. D. Li, Int. J. Quantum Chem. **111**, 4418 (2011).
[29] W. Z. Yao, D. Z. Li, and S. D. Li, J. Comput. Chem. **32**, 218 (2011).
[30] D. Yu. Zubarev, J. Li, L. S. Wang, and A. I. Boldyrev, Inorg. Chem. **45**, 5269 (2006).
[31] For selected reviews, see K. P. Hall and D. M. P. Mingos, Prog. Inorg. Chem. **32**, 237 (1984); P. G. Jones, Gold Bull. **14**, 102 (1981); **14**, 159 (1981); **16**, 114 (1983); **19**, 46 (1986).
[32] A. N. Alexandrova, E. Koyle, and A. I. Boldyrev, J. Mol. Model. **12**, 569 (2006).
[33] L. S. Wang, H. S. Cheng, and J. Fan, J. Chem. Phys. **102**, 9480 (1995).
[34] L. S. Wang and H. Wu, in *Advances in Metal and Semiconductor Clusters, Vol. 4, Cluster Materials*, edited by M. A. Duncan (JAI, Greenwich, CT, 1998), pp. 299–343.
[35] L. S. Wang and X. Li, in *Clusters and Nanostructure Interfaces*, edited by P. Jena, S. N. Khanna, and B. K. Rao (World Scientific, New Jersey, 2000), pp. 293–300.
[36] M. Saunders, J. Comput. Chem. **25**, 621 (2004); P. P. Bera, K. W. Sattelmeyer, M. Saunders, and P. v. R. Schleyer, J. Phys. Chem. A **110**, 4287 (2006).
[37] J. P. Perdew, K. Burke, and M. Ernzerhof, Phys. Rev. Lett. **77**, 3865 (1996).
[38] P. J. Hay and W. R. Wadt, J. Chem. Phys. **82**, 299 (1985).
[39] M. E. Casida, C. Jamorski, K. C. Casida, and D. R. Salahub, J. Chem. Phys. **108**, 4439 (1998); R. Bauernschmitt and R. Ahlrichs, Chem. Phys. Lett. **256**, 454 (1996).
[40] J. Cizek, Adv. Chem. Phys. **14**, 35 (1969); G. E. Scuseria and H. F. Schaefer, J. Chem. Phys. **90**, 3700 (1989); R. J. Bartlett and M. Musial, Rev. Mod. Phys. **79**, 291 (2007).
[41] M. J. Frisch, G. W. Trucks, H. B. Schlegel *et al.*, GAUSSIAN 09, Revision A.2, Gaussian, Inc., Wallingford, CT, 2009.
[42] Due to spectral overlap between bands X and A (Fig. 1), an unambiguous assignment of the first VDE is not possible. The quoted value may be considered tentative.
[43] See supplementary material at http://dx.doi.org/10.1063/1.4792501 for alternative optimized structures for $B_6Au_n^-$ and B_6Au_n ($n = 1-3$) at the PBE/Au/SDD/B/6-311++G(d,p) level of theory (Figs. S1–S6); molecular orbital pictures for the global minimum anion structures (**1**–**3**; Figs. S7–S9); and the global minimum anion structures and relevant neutral structures along with their bond distances (Fig. S10).
[44] L. S. Cederbaum, J. Phys. B **8**, 290 (1975); W. von Niessen, J. Schirmer, and L. S. Cederbaum, Comput. Phys. Rep. **1**, 57 (1984); V. G. Zakrzewski and W. von Niessen, J. Comput. Chem. **14**, 13 (1993); V. G. Zakrzewski and J. V. Ortiz, Int. J. Quantum Chem. **53**, 583 (1995).
[45] For a review, see J. V. Ortiz, V. G. Zakrzewski, and O. Dolgunitcheva, in *Conceptual Trends in Quantum Chemistry*, edited by E. S. Kryachko (Kluver, Dordrecht, 1997), Vol. 3, p. 463.
[46] A. I. Boldyrev, private communication.
[47] W. L. Li, C. Romanescu, T. Jian, and L. S. Wang, J. Am. Chem. Soc. **134**, 13228 (2012).
[48] The analyses of chemical bonding in $B_6Au_n^-$ and B_6Au_n ($n = 1-3$) in terms of aromaticity, antiaromaticity, and conflicting aromaticity appear to be solid for the following reasons: (i) the nature of double (π and σ) antiaromaticity in B_6^{2-} and B_6^- is a well-established concept in the literature,[11,16] and the Hückel ($4n + 2$) and $4n$ rules are among the most powerful and reliable criteria for aromaticity and antiaromaticity for such relatively simple systems. (ii) Delocalized π and σ bonding in $B_6Au_n^-$ and B_6Au_n ($n = 2, 3$) closely parallels that in the $B_7Au_2^-$ cluster,[25] which is recently shown to be of conflicting aromaticity: π antiaromatic and σ aromatic. (iii) Adaptive natural density partitioning (AdNDP) analyses on isovalent $B_6H_n^-$ and B_6H_n ($n = 2, 3$) clusters reach similar conclusions in terms of conflicting aromaticity.[46]

[49]For example, as shown in Fig. S7 for B_6Au^- (**1**) in the supplementary material,[43] HOMO−7 through HOMO−11 are primarily Au d^{10} lone-pairs in nature, whereas the set of bonding, partial bonding, and antibonding orbitals (HOMO−2, HOMO−4, and HOMO−12 through HOMO−15) can be effectively localized as six peripheral B−B single bonds.

[50]The NBO charges on the Au(B) atoms within the B−Au bonds show very little charge polarization: −0.045(−0.23), −0.024(−0.22), and −0.015(−0.19)/+0.051(−0.45)/+0.18(−0.45, −0.15) for the anions **1**−**3**, respectively, and +0.20(−0.12), +0.16(−0.05), and +0.14(−0.14)/+0.21(−0.20)/+0.49(−0.20, −0.12) for the neutrals **4**−**6**. In short, the NBO charges in the anion clusters range from −0.045 to +0.051 for terminal Au and +0.18 for bridging Au; whereas those in the neutrals range from +0.14 to +0.21 for terminal Au and +0.49 for bridging Au. These values are generally in line with the Wiberg bond orders, further indicating the highly covalent nature of the B−Au bonds.

[51]A. Ricca and C. W. Bauschlicher, Jr., J. Chem. Phys. **106**, 2317 (1997).

[52]D. Z. Li, Q. Chen, Y. B. Wu, H. G. Lu, and S. D. Li, Phys. Chem. Chem. Phys. **14**, 14769 (2012).

[53]H. J. Zhai, L. M. Wang, S. D. Li, and L. S. Wang, J. Phys. Chem. A **111**, 1030 (2007).

[54]H. J. Zhai, S. D. Li, and L. S. Wang, J. Am. Chem. Soc. **129**, 9254 (2007); S. D. Li, H. J. Zhai, and L. S. Wang, *ibid.* **130**, 2573 (2008); W. Z. Yao, J. C. Guo, H. G. Lu, and S. D. Li, J. Phys. Chem. A **113**, 2561 (2009); Q. Chen, H. J. Zhai, S. D. Li, and L. S. Wang, J. Chem. Phys. **137**, 044307 (2012).

[55]H. J. Zhai, J. C. Guo, S. D. Li, and L. S. Wang, ChemPhysChem **12**, 2549 (2011).